Transactions of the Korean Nuclear Society Autumn Meeting
Gyeongju, Korea, October 29-30, 2026

Error Analysis of Single-Pass Depletion Calculations for a Physics-Constrained Loss in AI-Based Core Surrogate Models

Jungseok Kwon [a*], Tongkyu Park [a], Byeong-hyeok Ha [a], Sung-kyun Zee [b]
[a]*FNC Technology, Heungdeok IT Valley Bldg. 32F, 13, Heungdeok 1-ro, Giheung-gu, Yongin-si, 16954, Korea*
[b]*FNC Technology, Daeduk Tech Business Center, 1004-2, 593, Daedukdae-ro, Yusung-gu, Daejeon-si, 34112, Korea*

[*]*Corresponding author: jskwon@fnctech.com*

Keywords : AI, Surrogate Model, Optimization, Reactor Physics, Depletion, i-SMR

1. Introduction

Loading pattern optimization is the process of determining the arrangement of fuel assemblies within a reactor core to meet safety and operational requirements. To support engineers in making design decisions, metaheuristic optimization methods have been developed [1-2]. More recently, AI-based surrogate models have been introduced to accelerate this process by replacing nodal neutronic calculations during the optimization [3-4].

In our previous work[4], we developed in AI-based core surrogate model to predict the core state at a specific state point. To extend this surrogate model to cover the entire depletion interval, a recursive one-step prediction approach is required. This approach necessitates updating the macroscopic cross-sections, which are assembled from nuclide number densities, at each burnup step to account for the changing nuclide composition. The updated macroscopic cross-sections then serve as inputs to the neural network for predicting the subsequent burnup step. One major issue in such recursive prediction is the accumulation of errors over successive steps. If the update is sorely based on data-driven learning, its accuracy suffers in data-sparse regions and when extrapolated beyond the training domain. To overcome this limitation, we plan to incorporate depletion equations as an auxiliary physics-based loss term that complements the data-driven training, rather than replacing it.

Ideally, this loss formulation should employ the same depletion method used to generate the reference solutions. While the reference data in this study is provided by the ASTRA[5] using a predictor-corrector method, reproducing this procedure is difficult within a single forward pass of a neural network. Therefore, a simplified single-pass depletion calculation is adopted for the loss formulation. In this approach, the depletion equations for the coupled chains of actinides and fission products are represented in a single depletion matrix and solved by the matrix exponential without the predictor-corrector method, with the neutron flux and microscopic cross sections held constant at their beginning of interval values.

Accordingly, as a preliminary step toward extending the surrogate model to full-cycle analysis (from BOC to EOC), this paper investigates the feasibility of employing the single-pass depletion calculation as such an auxiliary loss, and examines its error characteristics with respect to the burnup step size. The results thereby establish a basis for determining the appropriate burnup interval discretization when constructing the training dataset.

To evaluate this, the number densities computed by the simplified depletion equations were compared against ASTRA reference calculations using burnup step sizes of 100, 250, and 500 MWD/MTU, with a cumulative burnup of 5,000 MWD/MTU. For the cumulative error assessment, the number densities of U-235, U-238, I-135, Xe-135, and Gd were computed sequentially by applying the computed values from each interval as the initial conditions for the next. These sequential results were then compared with the ASTRA reference solutions.

2. Methods

The nuclide number densities were updated by solving the depletion equations once per burnup interval, without using the predictor-corrector approach, and the results were compared against the ASTRA reference solutions. This comparison is intended to identify the inherent error for each burnup step size. This error arises not from the formulas themselves, but from the approximation of freezing the neutron flux and cross sections at their values at the beginning of each interval.

The number densities at each burnup step were evaluated based on the depletion chains, with different treatments applied to each nuclide group. The actinide chain was solved using a matrix exponential of the depletion matrix, the number densities of I-135 and Xe-135 were evaluated from their chain at the equilibrium state, and the gadolinium isotopes were collapsed into a single effective Gd isotope whose depletion follows the chain-based effective model[6].

The reference solutions were generated with ASTRA by constructing an input deck for a soluble-boron-free core based on the i-SMR design data, which was depleted at rated power (100%) from BOC to a core-average

burnup of 5,000 MWD/MTU. The sensitivity of the error to the interval size was examined using three burnup step sizes of 100, 250, and 500 MWD/MTU. Because the depletion equations require a time variable, the core-average burnup increment was converted into an effective time step using the initial uranium loading and thermal power ($dt = dBU \times M_U/P_{th}$). These three intervals correspond to approximately 3.92, 9.81, and 19.61 days, respectively. At the beginning of each interval, the two-group neutron flux, node burnup, fuel and moderator temperatures, and moderator density were extracted from the ASTRA results. Using these state parameters, the corresponding two-group microscopic cross sections were interpolated from the cross-section tables and subsequently fed into the depletion formulas.

Two error metrics were defined for the evaluation. The first is the interval-wise one-step error, which quantifies the error introduced by a single application of the depletion equations. For this metric, the number densities at the beginning of each interval were taken from the ASTRA solutions. The depletion equations were then applied once, and the resulting number densities at the end of the interval were compared against the ASTRA reference solutions.

The second is the cumulative error, which quantifies the error accumulated over successive intervals. Starting from the initial ASTRA number densities, the number densities computed by the depletion equations in each interval were used as the initial conditions for the next burnup interval. This sequential calculation was repeated up to 5,000 MWD/MTU, and the resulting number densities at each burnup point were compared against the ASTRA solutions.

2.1 Depletion of Actinides and Pm/Sm Fission Products

For the actinides and the Pm/Sm fission products, the neutron flux and microscopic cross sections were frozen at their values at the beginning of each burnup interval. Under this assumption, the depletion equations were solved in closed form using the matrix exponential, and the number densities at the end of the interval were obtained without numerical time integration. The tracked nuclides and their transitions follow the depletion chain implemented in ASTRA (Fig. 1). The chain was not linearized, and all coupled transitions were instead represented in a single depletion matrix so that nuclides with multiple precursors are handled directly.

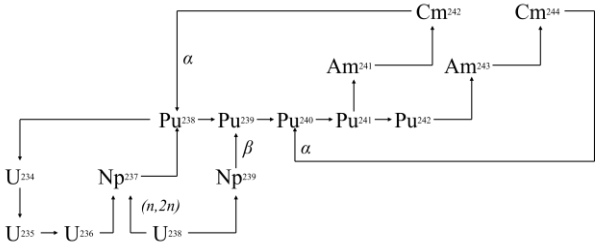


Fig. 1. Depletion chain of actinides

This matrix includes the twelve actinides (U-234, U-235, U-236, Np-237, U-238, Pu-238, Np-239, Pu-239, Pu-240, Pu-241, Pu-242, and Am-243) together with the five samarium-chain fission products (Pm-147, Pm-148, Pm-148m, Pm-149, and Sm-149), which are thus tracked as a single system of depletion equations. The actinides are linked by neutron capture, the beta decay of Np-239, the (n,2n) reaction of U-238, and the alpha decay of Pu-238, while the Pm/Sm nuclides are linked to the actinides through fission-yield production and to one another through capture and decay.

$$\frac{dN_i}{dt} = \sum_{i'} P_{i' \to i} N_{i'} - R_i N_i \qquad (1)$$

Writing the above equations for all tracked nuclides in vector form gives $dN/dt = \boldsymbol{A}N$, where $\boldsymbol{A}$ is the depletion matrix whose diagonal elements are -R_i and whose off-diagonal elements are $P_{i' \to i}$.

With $\boldsymbol{A}$ constructed from the values at the beginning of the interval and held constant over the interval, the number densities at the end of the interval are given by

$$\mathrm{N}(t + \Delta t) = \exp\,(\boldsymbol{A}\,\Delta t)\,\mathrm{N}(t) \qquad (2)$$

The matrix form directly handles nuclides with multiple precursors. The evaluation of $\exp(\boldsymbol{A}\,\Delta t)$ proceeds in the following steps for each node and interval:

1. The two-group neutron flux, node burnup, fuel and moderator temperatures, and moderator density at the beginning of the interval are taken from the ASTRA solution.
2. The two-group microscopic capture, fission, and (n,2n) cross sections of each nuclide are interpolated from the cross-section tables at that state.
3. The reaction rates ($\sum_g \sigma_{\{x,g,i\}\phi_g}$) are combined with the decay constants, branching ratios, and fission yields to fill the elements of $\boldsymbol{A}$.
4. The matrix exponential ($\exp(\boldsymbol{A}\Delta t)$) is evaluated once using the expm function of the SciPy library, which implements a scaling-and-squaring algorithm with Padé approximation [7].
5. The resulting transition matrix is multiplied by the number densities at the beginning of the interval to give the number densities at the end of the interval.

2.2 Equilibrium Equations for I-135 and Xe-135

For I-135 and Xe-135, the equilibrium equations were used instead of the time-dependent depletion equations. Under constant rated-power operation, Xe-135 reaches equilibrium within approximately two days, which is shorter than the finest burnup interval considered in this study (3.92 days). The reference solutions were therefore generated under the equilibrium-xenon condition, and the number densities of both nuclides were calculated from the equilibrium equations using the physical quantities at the end of each interval.

$$N_{\mathrm{I}} = \frac{\gamma_{\mathrm{I}} \sum_g \Sigma_{f,g} \phi_g}{\lambda_{\mathrm{I}}}, \quad (3)$$

$$N_{\mathrm{Xe}} = \frac{\lambda_{\mathrm{I}} N_{\mathrm{I}} + \gamma_{\mathrm{Xe}} \sum_g \Sigma_{f,g} \phi_g}{\lambda_{\mathrm{Xe}} + \sum_g \sigma_{a,\mathrm{Xe},g} \phi_g} \quad (4)$$

All quantities were evaluated at the end of the interval. The macroscopic fission cross sections were assembled from the number densities computed in Section 2.1 and the corresponding microscopic fission cross sections.

2.3 Effective Depletion Model for Gadolinium

For the gadolinia burnable absorber, the microscopic absorption cross sections of Gd-155 and Gd-157 change rapidly and non-linearly with burnup, making interpolation from the cross-section tables inaccurate. Therefore, instead of tracking the individual isotopes, an effective Gd number density that lumps the five isotopes from Gd-154 to Gd-158 into a single nuclide was tracked [6]. The effective number density and the corresponding effective absorption cross section are defined as;

$$N_{\mathrm{Gd}}^{\mathrm{eff}} = 5N_{154} + 4N_{155} + 3N_{156} + 2N_{157} + N_{158}, \quad (5)$$

$$\sigma_{a,g}^{\mathrm{eff}} = \frac{\sum_{m=154}^{158} N_m \sigma_{a,g,m}}{N_{\mathrm{Gd}}^{\mathrm{eff}}} \quad (6)$$

Where, the weights in Eq. (5) depend only on the structure of the depletion chain. Because the effective absorption cross section varies almost linearly with burnup, it can be accurately evaluated by table interpolation. In this work, both quantities were therefore used directly in their lumped form, without evaluating the individual isotopes. The effective cross section was interpolated from the cross-section library, and the effective number density was taken from the ASTRA solution.

Since the effective Gd has no production source and is removed only by neutron absorption, its depletion equation reduces to

$$\frac{dN_{\mathrm{Gd}}^{\mathrm{eff}}}{dt} = -N_{\mathrm{Gd}}^{\mathrm{eff}} \sum_g \sigma_{a,g}^{\mathrm{eff}} \phi_g \quad (7)$$

With the neutron flux and the effective cross section frozen at their values at the beginning of each burnup interval, the number density at the end of the interval is given by the exponential decay formula

$$N_{\mathrm{Gd}}^{\mathrm{eff}}(t + \Delta t) = N_{\mathrm{Gd}}^{\mathrm{eff}}(t) \exp\left(-\sum_g \sigma_{a,g}^{\mathrm{eff}} \phi_g \Delta t\right) \quad (8)$$

3. Results

The errors reported in this section are the node-wise relative errors of the number densities with respect to the ASTRA reference solutions. For the one-step errors, the relative error was computed at every fuel node and burnup interval, and the maximum was taken over all nodes and intervals. For the cumulative errors, the relative error was computed at every fuel node and burnup point along the sequential calculation.

3.1 One-Step Errors of the Actinides and Pm/Sm Fission Products

Table I summarizes the maximum relative errors of the 17 nuclides tracked in Section 2.1 over all burnup intervals and fuel nodes. The errors increase with the burnup step size, because the depletion operator constructed at the beginning of the interval is held fixed over a longer period. Since these are independent one-step results, no accumulation effect is included.

Table I: . Maximum one-step errors of the number densities for each burnup step size (0–5,000 MWD/MTU).

Nuclide	100	250	500
U-234	1.59%	8.99%	31.1%
U-235	5.40×10^{-3}%	0.0149%	0.0387%
U-236	0.733%	1.13%	1.78%
Np-237	0.690%	0.926%	1.84%
U-238	1.88×10^{-4}%	3.72×10^{-4}%	9.99×10^{-4}%
Pu-238	1.34%	1.82%	3.50%
Np-239	0.613%	1.51%	2.95%
Pu-239	0.378%	1.34%	1.27%
Pu-240	1.14%	2.10%	3.46%
Pu-241	1.65%	3.22%	5.20%
Pu-242	1.57%	2.19%	7.40%
Am-243	0.766%	0.908%	1.63%
Pm-147	0.743%	1.18%	1.83%
Pm-148m	1.53%	2.20%	3.38%
Pm-148	1.69%	2.50%	4.78%
Pm-149	1.41%	2.50%	4.04%
Sm-149	0.887%	1.02%	1.14%

3.2 Errors of the Equilibrium Model for I-135 and Xe-135

Table II presents the errors of the equilibrium I-135 and Xe-135 number densities evaluated at the end of each interval. Because the equilibrium number densities are algebraic functions of the instantaneous core state, the errors are practically independent of the burnup step size and remain below 0.34%.

Table II. Errors of the equilibrium I-135 and Xe-135 number densities for each burnup step size.

Nuclide	100	250	500
I-135	0.336%	0.329%	0.334%
Xe-135	0.264%	0.261%	0.270%

3.3 Errors of the Effective Depletion Model for Gadolinium

Table III summarizes the maximum one-step errors of the effective Gd number density, evaluated over the gadolinia nodes for each burnup interval. Because the effective absorption cross section varies smoothly with burnup, the errors are two to three orders of magnitude smaller than those of the other nuclides, remaining below 3.84×10^{-2}% even for the 500 MWD/MTU step size.

Table III. Maximum one-step errors of the effective Gd number density for each burnup step size (0–5,000 MWD/MTU).

Nuclide	100	250	500
Effective Gd	3.65×10^{-3}%	1.21×10^{-2}%	3.84×10^{-2}%

3.4 Cumulative Errors up to 5,000 MWD/MTU

Table IV compares the cumulative errors obtained by propagating the estimated number densities through subsequent intervals up to 5,000 MWD/MTU, with burnup step sizes of 100 and 500 MWD/MTU. Since the core consists of fresh fuel at BOC, the comparison focuses on the nuclides present in the fresh fuel, specifically U-235, U-238, and the effective gadolinium, as well as I-135 and Xe-135 as determined by the equilibrium equations. The values in Table IV represent the maximum relative errors across all burnup points and fuel nodes during the propagation.

Table IV. Maximum cumulative errors of the number densities (0–5,000 MWD/MTU).

Nuclide	100	500
U-235	0.168%	0.224%
U-238	7.00×10^{-4}%	2.07×10^{-3}%
I-135	0.325%	0.326%
Xe-135	0.254%	0.264%
Effective Gd	0.125%	0.274%

3. Conclusions

This paper assessed the feasibility of a single-pass depletion calculation for updating nuclide number densities, as a preliminary step toward extending the AI-based core surrogate model to full-cycle analysis. The single-pass formulation was used since the multi-step predictor-corrector procedure could not be directly incorporated into a loss function evaluated in a single forward pass. Accordingly, the purpose of this study was not to match the ASTRA solutions exactly, but rather to quantify the error contributed by a single application of the depletion equations as a function of the burnup step size. The actinide and Pm/Sm chains were solved using the matrix exponential of a single depletion matrix, I-135 and Xe-135 were evaluated using their equilibrium equations; and the gadolinia burnable absorber was treated with the effective Gd depletion model. The results were compared with the ASTRA reference solutions for burnup step sizes of 100, 250, and 500 MWD/MTU, up to a core-average burnup of 5,000 MWD/MTU.

The one-step errors of the directly tracked nuclides increased with the burnup step size and remained within a few percent for the major nuclides, while the trace nuclide U-234 showed considerably larger errors. The equilibrium I-135 and Xe-135 errors were practically independent of the step size and stayed below 0.34%, and the effective Gd errors were two to three orders of magnitude lower than those for the other nuclides. Even with a step size of 500 MWD/MTU, the errors of the fresh-fuel nuclides and equilibrium-treated nuclides remained below 0.33% in the cumulative evaluation up to 5,000 MWD/MTU. These findings show that the single-pass depletion calculation maintains adequate accuracy for the major nuclides across the burnup step sizes evaluated, and they serve as a basis for establishing the burnup interval discretization when constructing the training dataset. These errors arise from applying the depletion equations once per interval without using the predictor-corrector approach, and they vary depending on the burnup step size. The remaining discrepancy from the ASTRA solutions is expected to be decreased via the data-driven training.

Acknowledgements This work was supported by the Innovative Small Modular Reactor Development Agency grant funded by the Korea Government (MOTIE) (RS-2023-00259289)

REFERENCES

[1] Stevens, J. G., Smith, K. S., Rempe, K. R., and Downar, T. J., “Optimization of Pressurized Water Reactor Shuffling by Simulated Annealing with Heuristics,” Nuclear Science and Engineering, 121, 67–88 (1995).
[2] T. Park, et al., “Multi objective loading pattern optimization by simulated annealing employing discontinuous penalty function and screening technique”, Nuclear Science and Engineering, 162(2), 134-147 (2009).
[3] S. Jeong and H. C. Lee, “Loading Pattern Optimization for OPR-1000 by Simulated Annealing with a Screening Technique using Pin-wise Vision Transformer Model,” Transactions of the Korean Nuclear Society Spring Meeting, Jeju, Korea, May 22–23, 2025.
[4] J. Kwon, T. Park, and S.K. Zee, “AI-Based Prediction Module of Key Neutronic Characteristics to Optimize Loading Pattern for i-SMR with Flexible Operation”, Korean J. Chem. Eng., 41, 2741–2759 (2024)
[5] Yoon, J. I., Park, S. W., and Park, H. S., “Verification & Validation of KARMA/ASTRA with Benchmark and Core-Follow Analyses,” Transactions of the American Nuclear Society, 105, 801–802 (2011).
[6] J. Choe, S. Choi, and D. Lee, “Analysis of Effective Gadolinium Depletion Model”, Transactions of the Korean Nuclear Society Spring Meeting, Jeju, Korea, May 17–18, 2018.
[7] P. Virtanen et al., "SciPy 1.0: Fundamental Algorithms for Scientific Computing in Python," Nature Methods 17, 261–272 (2020)